

Published in final edited form as:

ACS Chem Biol. 2017 October 20; 12(10): 2631–2643. doi:10.1021/acscchembio.7b00694.

BTN3A1 discriminates $\gamma\delta$ T cell phosphoantigens from non-antigenic small molecules *via* a conformational sensor in its B30.2 domain

Mahboob Salim^{#1}, Timothy J Knowles^{#2}, Alfie T. Baker^{#1}, Martin S. Davey¹, Mark Jeeves³, Pooja Sridhar², John Wilkie⁴, Carrie R. Willcox¹, Hachemi Kadri⁵, Taher E. Taher¹, Pierre Vantourout^{6,7}, Adrian Hayday^{6,7}, Youcef Mehellou⁵, Fiyaz Mohammed^{1,*}, and Benjamin E. Willcox^{1,*}

¹Institute of Immunology and Immunotherapy, University of Birmingham, Edgbaston, Birmingham, UK, B15 2TT

²School of Biosciences, University of Birmingham, Edgbaston, Birmingham, UK, B15 2TT

³Institute of Cancer and Genomics, Henry Wellcome Building for Biomolecular NMR, University of Birmingham, Edgbaston, Birmingham, UK

⁴School of Chemistry, University of Birmingham, Edgbaston, Birmingham, UK, B15 2TT

⁵Cardiff School of Pharmacy and Pharmaceutical Sciences, King Edward VII Avenue, Cardiff University, Cardiff CF10 3NB, UK

⁶Peter Gorer Department of Immunobiology, King's College London, London SE1 9RT, UK

⁷The Francis Crick Institute, London NW1 1AT, UK

These authors contributed equally to this work.

Abstract

Human V γ 9/V δ 2 T-cells detect tumour cells and microbial infections by recognising small phosphorylated prenyl metabolites termed phosphoantigens (P-Ag). The type-1 transmembrane protein Butyrophilin 3A1 (BTN3A1) is critical to the P-Ag-mediated activation of V γ 9/V δ 2 T-cells, however, the molecular mechanisms involved in BTN3A1-mediated metabolite sensing are unclear, including how P-Ag are discriminated from non-antigenic small molecules. Here, we utilised NMR and X-ray crystallography to probe P-Ag sensing by BTN3A1. Whereas the BTN3A1 Immunoglobulin Variable domain failed to bind P-Ag, the intracellular B30.2 domain bound a range of negatively-charged small molecules, including P-Ag, in a positively-charged surface pocket. However, NMR chemical shift perturbations indicated BTN3A1 discriminated P-Ag from non-antigenic small molecules by their ability to induce a specific conformational change

*Corresponding author b.willcox@bham.ac.uk or f.mohammed@bham.ac.uk.

Author contributions

MS, TJK, MSD, PV, AH, YM, FM and BEW planned and organised the experiments. MS, ATB, PS performed purification experiments. FM, ATB and MS carried out crystallisation trials, X-ray diffraction experiments, structure determination and analysis. MS, TJK, ATB and MJ conducted NMR experiments and analysis. ATB, MSD, CRW and TET performed T cell culture and activation assays. JW, HK and YM conducted molecular modelling studies. PV generated the BTN3A1 Knock-out HEK293T cell line. ATB performed BTN3A1 mutagenesis and V δ 2⁺ activation assays. ATB, MSD, CRW, YM, FM and BEW wrote the manuscript.

in the B30.2 domain that propagated from the P-Ag binding site to distal parts of the domain. These results suggest BTN3A1 selectively detects P-Ag intracellularly *via* a conformational antigenic sensor in its B30.2 domain, and have implications for rational design of antigens for V γ 9/V δ 2 -based T-cell immunotherapies.

Keywords

Butyrophilin; phosphoantigen; B30.2; conformational change; $\gamma\delta$ T cell receptor; P-Ag (phosphoantigens)

Introduction

V γ 9/V δ 2 T cells represent the dominant subtype of human $\gamma\delta$ T cells in adult peripheral blood (1). Present since birth (2), this subset expands in response to a number of different infections, including tuberculosis, leprosy, typhoid, malaria, and toxoplasmosis, and studies in primate models have suggested a role in immunity to *Mycobacterium tuberculosis* (3). In addition, they are also capable of *in vitro* recognition of a diverse range of cancer cells (1). Target cell recognition is dependent on their V γ 9/V δ 2 T cell receptor (TCR) (4), and is also cell-cell contact-dependent, but is MHC-independent (5, 6). V γ 9/V δ 2 T cells display potent effector capacity, including cytotoxicity and production of IFN- γ and TNF α (7, 8). Based on their universal presence in humans, proliferative capacity, potential implication in both pathogen-specific and tumour-specific immunity, MHC-unrestricted target cell recognition, and pharmacological manipulability (see below), V γ 9/V δ 2 T cells have become the dominant focus for therapeutic exploitation of $\gamma\delta$ T cells (9).

Unlike classical $\alpha\beta$ T cells, V γ 9/V δ 2 T cells are activated by non-peptidic pyrophosphate (diphosphate) antigens (P-Ag), of which the first to be identified was isoprenyl pyrophosphate/diphosphate (IPP) (10), a compound all organisms, including humans, use to synthesise isoprenoid compounds, and which in eukaryotes is generated *via* the mevalonate and non-mevalonate pathways. However, the second non-mevalonate or MEP pathway utilised by most eubacteria, some protozoa and cyanobacteria but not humans, generates hydroxy-3-methyl-but-2-enyl pyrophosphate/diphosphate (HMBPP) (11), a potent stimulator of V γ 9/V δ 2 T cell responses. The ~30,000 increased potency of HMBPP over IPP suggests that in normal situations it may enable V γ 9/V δ 2 T cells to distinguish exogenous microbial (7) from endogenous host P-Ag(10). However, a number of studies have highlighted spontaneous recognition of cancer cell lines by V γ 9/V δ 2 T cells (5, 12), a phenomenon that likely relates to increased IPP levels in such cells (8). Moreover, pharmacological inhibitors of IPP catabolism, including clinically used aminobisphosphonates such as Zoledronate (13–15), are known to sensitize target cells, including cancer cells, for V γ 9/V δ 2 T cell recognition *via* accumulation of IPP. Therefore, uniquely for a T cell subset, the antigen-driven effector responses of V γ 9/V δ 2 T cells are pharmacologically manipulable.

Despite being the subject of strong therapeutic interest, V γ 9/V δ 2 T cells recognise target cells *via* a TCR- and P-Ag-dependent mechanism the details of which remain largely unclear. One important advance has been the identification of the butyrophilin-like molecule

BTN3A1 as a critical mediator of P-Ag sensing (16, 17). BTN3A1 is a type 1 transmembrane protein consisting of an ectodomain comprising a membrane distal variable-like domain, a membrane proximal constant-like immunoglobulin domain, a single transmembrane spanning region, and an intracellular B30.2 domain (Figure S1a) (18, 19). Nevertheless, opposing mechanisms have been proposed to explain how BTN3A1-mediated P-Ag sensing takes place. Based partly on crystallographic data, Vavassori *et al* suggested direct presentation of P-Ag including IPP and HMBPP to V γ 9/V δ 2 T cells by the membrane-distal variable-like domain within the BTN3A1 ectodomain (17). In contrast, a number of studies have instead proposed that BTN3A1 acts as an intracellular P-Ag sensor, initiated by P-Ag binding to the intracellular B30.2 domain of BTN3A1 (19–21). Despite these studies, the molecular events proximal to P-Ag interaction are entirely unclear.

Understanding the molecular mechanisms underlying BTN3A1's role in P-Ag sensing will enhance understanding of V γ 9/V δ 2 T cell recognition and could suggest novel immunotherapeutic strategies. In this study, we present data that suggest BTN3A1 acts as an intracellular metabolite sensor capable of triggering downstream activation events *via* a conformational change in its cytosolic B30.2 domain, which occurs selectively in response to P-Ag but not non-antigenic small molecules (Figure S1b).

Results and Discussion

Antigenic pyrophosphates selectively bind to the B30.2 domain of BTN3A1

Since the mode of P-Ag interaction with BTN3A1 has been controversial (17, 20) we first sought to test if we could detect P-Ag binding to the BTN3A1 IgV-like domain, and to the B30.2 domain, as well as locate the identity of putative binding sites. We applied nuclear magnetic resonance (NMR) studies to test interaction of P-Ag with the membrane-distal Variable-like domain of BTN3A1, and separately, with the intracellular B30.2 domain. NMR provided a powerful methodology not only to confirm interaction, but also potentially to map sites of interaction on the protein surface. First, the IgV-domain was expressed in *E. coli* and subjected to ^1H - ^{15}N NMR in the absence and presence of HMBPP and the more stable phosphonate analogue, cHDMAPP (22). High quality spectra were detected, which allowed us to assign all residues in the ^1H - ^{15}N HSQC spectrum of the IgV domain, including those purported to bind HMBPP/IPP based on a previous crystallographic study (17). However, despite the use of relatively high P-Ag concentrations (1.5 mM), we failed to identify any chemical shift perturbations in the presence of HMBPP (Figure 1) or cHDMAPP (Figure S2). This included residues in the proposed P-Ag binding site, for which well resolved peaks in the HSQC spectra were observable both in the absence and presence of P-Ag. This indicated a lack of interaction of biologically highly potent P-Ag with BTN3A1 IgV-like domain, including residues E64, K66, R88, Y127, Q129 and Y134 (residue numbering is based on Uniprot accession code O00481) previously highlighted by Vavassori and colleagues as interacting with IPP/HMBPP.

We then tested P-Ag interaction with the B30.2 domain of BTN3A1, employing a similar NMR-based approach, using B30.2 protein recombinantly expressed in ^1H - ^{15}N -labelled form in *E. coli*. In contrast to analyses with the V-like domain, ^1H - ^{15}N NMR experiments using the intracellular B30.2 domain indicated substantial chemical shift changes in

numerous B30.2 residues in the presence of P-Ag, indicating direct interaction (Figure 2, Figure S3). Notably, broadly similar chemical shift perturbations were observed with HMBPP (Figure S3a) and cHDMAPP (Figure 2). In contrast, smaller chemical shift perturbations were observed following titration with IPP (Figure S3b). Collectively, these studies confirmed that P-Ag selectively bind to the intracellular B30.2 domain, but do not bind to the extracellular IgV-like domain.

The B30.2 domain is capable of binding negatively charged small molecules

To understand the structural basis of P-Ag/B30.2 interaction, we attempted to crystallise the B30.2 domain with cHDMAPP, exploring co-crystallisation strategies and a wider range of crystallisation conditions than have previously been published (20). We obtained high quality crystals in a range of conditions that differed from previous structural analyses, and collected 1.6Å and 1.7Å diffraction data on crystals from two such conditions (Table S1). These showed unequivocal electron density for a small molecule moiety, in each case within a positively charged surface pocket, incorporating residues H381, R442, R448 and R499 (Figure 3a-d). However, early inspection of the electron density revealed a poor fit to HMBPP, whereas the density fitted closely to malonate and citrate, present in the crystallisation conditions for the 1.6Å and 1.7Å datasets respectively (Figure 3a-d). This confirmed that these structures represented serendipitous co-crystal structures of the B30.2 domain with malonate and citrate, neither of which has previously been highlighted as activating antigens for V γ 9V δ 2 T cells. Superimposition with the cHDMAPP-soaked and glutaraldehyde-cross linked structure of Sandstrom *et al* indicated that the bound malonate and citrate moieties overlapped strikingly with the proposed position of cHDMAPP (Figure 3e), appearing to interact with essentially the same electropositive surface patch on the B30.2 domain and mediating a network of hydrogen-bonding interactions with neighbouring B30.2 residues (Figure 3f-h).

Importantly, superimposition of these malonate and citrate B30.2 co-crystal structures with previous apo structures demonstrated strong similarities, with backbone rms deviations of 0.229Å (for 187 aligned C α atoms) and 0.171Å (for 187 aligned C α atoms), respectively (Figure 3i). In addition, very few conformational alterations were evident around the binding site, aside from minor adjustments in neighbouring side chains, although we could not formally discount the possibility that crystal contacts constrained possible conformational changes from being detected. These data proved unequivocally that the proposed HMBPP binding site within the B30.2 domain is able to bind a range of negatively charged small molecules, including the negatively charged small molecules malonate and citrate, which are not thought to activate V γ 9/V δ 2 T cells. However they raised the question of how antigenic *versus* non-antigenic small molecules are discriminated by the B30.2 domain.

B30.2 chemical shifts distinguish P-Ag from non-antigenic molecule binding

Previously it has been suggested that instead of being presented directly by the BTN3A1 IgV-like ectodomain, P-Ag may induce a conformational change in the B30.2 domain, based partly on the observation that B30.2 apo crystals soaked in cHDMAPP dissolved (20). To determine to what extent P-Ag and non-antigenic small molecules could induce conformational alterations in the B30.2 domain in solution, we used NMR to titrate each

ligand against the apo form of BTN3A1 B30.2 domain and analyse subsequent chemical shift perturbations. We then went on to map NMR chemical shifts observed in the B30.2 domain upon P-Ag binding (Figure 4), and compare them to those induced in the presence of malonate (Figure 5) and citrate (Figure S4). As highlighted above, extensive chemical shifts relative to the apo B30.2 were observed upon HMBPP/cHDMAPP exposure (Figure 2, Figure S3). Assignment of the ^1H - ^{15}N HSQC spectrum indicated that residues undergoing chemical shifts included several clustered close to the previously proposed P-Ag binding site (20). In addition, the detection of chemical shifts in residues protruding from the β 2- β 3 loop (K366 and Q369), β 5 strand (S413), β 3- β 4 loop (F390 and I391), β 5- β 6 loop (K419, G420 and N428), β 6 strand (G429 and W431) and the β 6- β 7 loop (G438), which were distal to this site, confirmed that P-Ag binding had induced conformational changes in the B30.2 domain that extended beyond the immediate P-Ag interaction site (Figure 4a-b). In comparison, IPP induced similar chemical shift perturbations as to those observed with HMBPP and cHDMAPP, although these shifts were qualitatively smaller in magnitude (Figure 4c).

In contrast, titration of the B30.2 domain with malonate and citrate revealed only a small number of chemical shift perturbations compared to the apo structure (Figure 5a, Figure S4a). In addition, these were small in magnitude, and in residues located close to the citrate/malonate binding site observed in crystallographic studies. However, unlike HMBPP/cHDMAPP, both malonate and citrate failed to induce perturbations in residues more distal to the proposed HDMAPP binding site, notably K366, Q369, F390, I391, S413, K419, N428, G429 and W431 (Figure 5b, Figure S4b). These data indicated that unlike P-Ag, alterations induced in B30.2 by citrate or malonate binding are restricted to regions close to the small molecule interaction site.

We next sought to directly confirm whether citrate and malonate were able to stimulate V γ 9/V δ 2 T cells or not. To do this, we compared the functional responsiveness of human peripheral blood V γ 9/V δ 2 T cells and CD8⁺ T cells (Figure 6a) to citrate, malonate and P-Ag indicated to bind the BTN3A1 B30.2 domain. While V γ 9/V δ 2 T cells responded to known P-Ags cHDMAPP and IPP (Figure 6b), neither citrate nor malonate were capable of stimulating the upregulation of T cell activation markers, CD25 and CD69 in V γ 9/V δ 2 T cells (23–25) (Figure 6c). Moreover, while CD8⁺ T cells showed no appreciable response to any molecule tested (Figure 6d), V γ 9/V δ 2 T cells required ~8000 fold less cHDMAPP ($\text{EC}_{50} = 1.2 \text{ nM}$) than IPP ($\text{EC}_{50} = 7783 \text{ nM}$) to induce similar activation levels of CD25 and CD69 (Figure 6e). Taken together, these data indicate that while a range of small molecules are able to bind the BTN3A1 B30.2 domain, only structures very closely related to the microbially-derived diphosphate antigen, HMBPP, appear capable of activating human V γ 9/V δ 2 T cells.

As neither malonate nor citrate resembles traditional P-Ags, we sought to investigate other potential ligands. The nucleotide Adenosine diphosphate (ADP; also known as Adeonsine pyrophosphate) is an important molecule in cellular metabolism and also has a role in activation of blood platelets. Similarly to HMBPP and IPP it contains a diphosphate headgroup, but differs in the hydrocarbon chain as it is linked to a pentose sugar and adenine nitrogenous base (Figure S1b). ^1H - ^{15}N HSQC experiments showed that ADP caused

widespread chemical shift perturbations on interaction with the B30.2 domain (Figure S5a), and when mapped these shifts were found to be around the previously proposed binding site in addition to the periphery of the molecule, suggesting that as for HMBPP or IPP, it also induced an overall conformational change (Figure S5b-c). We repeated our earlier experiments in order to assess the stimulatory capacity of ADP on V γ 9/V δ 2 T cells. However, unlike HMBPP or IPP, ADP was found to be incapable of activating V γ 9/V δ 2 T cells at a range of concentrations similar to citrate and malonate (Figure 6f). Further analysis of the chemical shift perturbations detected with the addition of ADP showed that a number of shifts occurred in a different direction compared to those with HMBPP or IPP, suggesting that the conformational change induced by ADP may be qualitatively different compared to that induced by HMBPP or IPP.

***In silico* modelling of small molecule interaction with the B30.2 domain**

The disparity between the activation potential of each diphosphate containing molecule suggests that the hydrocarbon tail is also important in inducing activation. To help rationalise interaction of small molecule binding to the B30.2 domain, we initially performed *in silico* docking of both cHDMAPP and IPP into the crystal structure of the B30.2 domain. Interestingly, both compounds were docked into the same site confirmed by the NMR studies as the site involved in binding negatively charged small molecules (Figure 7a-b). Indeed, the diphosphate headgroup of cHDMAPP and IPP was docked into the positively charged site and formed key interactions with three arginine residues (R442, R448 and R499). Intriguingly, the free hydroxyl group of cHDMAPP was predicted to form a hydrogen bond with H381, an interaction unique to cHDMAPP (Figure 7a) and not IPP as it lacks this free hydroxyl (Figure 7b). Notably, this interaction was not observed in the co-crystal structure of B30.2 with cHDMAPP as the organic chain lacked resolvable electron density (20). Subsequent similar *in silico* docking of malonate and citrate indicated that these compounds docked well into the positively charged pocket where the diphosphate head of HMBPP and IPP fitted (data not shown). Similar key residues within this pocket, namely R442 and R499, which the diphosphate group interacted with, also formed hydrogen bonds with the citrate and malonate ligands. Consistent with its status as the most potent V γ 9/V δ 2 T-cell activator, HMBPP showed a more favourable binding free energy (-15.57 kcal/mol) compared to IPP (-14.79 kcal/mol). Moreover, the binding free energies for citrate and malonate were considerably less favourable than either P-Ag (-9.79 kcal/mol and -7.67 kcal/mol, respectively), suggesting they may have a substantially reduced affinity.

To investigate the role of H381 and the neighbouring hydrophobic residue Y382 in the activation of V γ 9/V δ 2 T cells we generated a series of BTN3A1 B30.2 mutants, using site directed mutagenesis to substitute each residue for either an alanine or a similar amino acid (H381R and Y382F). Firstly, CRISPR/Cas9 empty vector HEK293T cells pulsed with zoledronate were capable of the activation of a short term V δ 2⁺ T cell line expanded from human PBMCs (Figure 8a). However, zoledronate pulsed CRISPR/Cas9 BTN3A1 knock-out HEK293T cells were unable to support activation of V δ 2⁺ T cells (Figure 8a). Reintroduction of wild type (WT) BTN3A1 by transient transfection into BTN3A1 knock-out HEK293T cells rescued zoledronate mediated V δ 2⁺ T cells activation (Figure 8a). Next, we expressed each mutant construct in BTN3A1 knock-out HEK293T cells treated with

Zoledronate and assessed V δ 2⁺ T cell activation (Figure 8b). We evaluated the abrogation of CD25 expression on V δ 2⁺ T cells by each BTN3A1-mutant through normalising the percentage of CD25⁺ V δ 2⁺ T cells to the wild-type BTN3A1 T cell response. This analysis revealed that H381A, H351R and Y382A reduced the activation of V δ 2⁺ T cells by >50% of that of WT BTN3A1. Interestingly, BTN3A1 H381R showed >90% reduction in V δ 2⁺ T cells activation to that of the WT BTN3A1, while the BTN3A1 Y382F mutant could support >60% of the activation observed for WT BTN3A1 (Figure 8c).

We then recombinantly expressed the B30.2 domain incorporating these mutations and analysed interactions with diphosphate ligands. ¹H-¹⁵N HSQC experiments confirmed that BTN3A1 B30.2 H381A, Y382A and Y382F were similarly folded, however BTN3A1 B30.2 H381R was remarkably unstable and quickly precipitated, and so was unsuitable for these experiments. We observed a difference when comparing H381A and Y382A to WT, in terms of chemical shift perturbations (Figure S6) upon P-Ag binding. Our *in silico* experiments had predicted that the interaction between B30.2 H381A and HMBPP would be reduced to levels comparable to IPP; however experimentally we observed greatly reduced chemical shift perturbations in terms of number and magnitude with both HMBPP and IPP. Similarly, Y382A also showed a reduction with IPP, however the shifts observed with HMBPP was relatively unaffected. In comparison, little change was seen in chemical shift perturbations induced in B30.2 Y382F, with some exceptions. These results may reflect differences between molecular components involved in initial P-Ag interaction and subsequent conformational rearrangements. Importantly, these experiments directly implicate pocket residues in mediating the specific conformational change triggered by P-Ag binding.

While BTN3A1 is now acknowledged to be a critical mediator of antigen recognition by V γ 9/V δ 2 T cells, the molecular basis by which it sensitizes P-Ag-exposed target cells for recognition by this T cell subset is still unclear (26). Studies published within the last 3 years have proposed opposing models. Vavassori *et al* presented crystal structures of the BTN3A1 IgV-like domain incorporating electron density supposedly matching IPP or HMBPP, combined with SPR data purporting to demonstrate interaction of a V γ 9/V δ 2 TCR with the BTN3A1 IgV, which only appeared to be marginally enhanced in affinity in the presence of IPP/HMBPP (17). However, Sandstrom *et al* challenged key elements of these findings, noting that the electron density purportedly representing IPP/HMBPP instead matched that of a crystallisation component, polyethylene glycol(20). In addition, Sandstrom *et al* failed to replicate TCR binding to the IgV-like domain, in the presence or absence of IPP/HMBPP, and instead presented evidence for P-Ag binding directly to the intracellular B30.2 domain. Also, subsequent studies by Wang et al and Rhodes et al have also supported an intracellular sensor function (19, 21). The aim of the current study was to shed light on the molecular events proximal to P-Ag interaction with BTN3A1.

Using NMR spectroscopy, we failed to detect any interaction of P-Ag with the IgV-like domain, despite detecting strong resonances for residues of the putative IPP/HMBPP binding site proposed by Vavassori *et al*. This casts further doubt on the findings of Vavassori *et al* (17). In contrast, we observed strong signals denoting direct interaction of P-Ag with the intracellular B30.2 domain, as evidenced by numerous chemical shifts upon P-Ag exposure. This strongly supports previous data (20, 27), confirming that P-Ags directly

interact with BTN3A1, and that this occurs solely *via* the B30.2 domain, and not *via* the IgV-like domain. Since the B30.2 domain is within the intracellular region of BTN3A1, this adds to the growing body of evidence that instead of ‘presentation of altered self’ by its IgV-like domain, the BTN3A1 B30.2 domain is a critical player in an intracellular sensing mechanism that translates cytosolic P-Ag exposure in target cells into the ability to stimulate V γ 9/V δ 2 T cells in a TCR-dependent manner (19–21).

Our study sheds significant light on the region of B30.2 involved in P-Ag binding. Previously, an electropositive surface patch on the B30.2 domain was highlighted as a putative P-Ag binding site by the ‘soaking’ of glutaraldehyde-crosslinked apo B30.2 domain crystals with cHDMAPP. Notably, the only interpretable electron density for the cHDMAPP moiety in this structure was the pyrophosphate headgroup. In addition, a recent extensive mutagenesis study of BTN3A1 highlighted the functional importance of a set of residues clustered around this putative site in P-Ag-mediated V γ 9V δ 2 activation (21). Our NMR data are consistent with this proposed binding site, since several of the chemical shifts we observed upon P-Ag binding cluster around this pocket. Indeed, several amino acids proximal to the site highlighted by Wang et al(21) as functionally important in P-Ag sensing underwent detectable chemical shifts upon P-Ag interaction (K423, R442, R448 and H378; additionally V384). In addition, our crystallography data provide unequivocal proof that the binding site proposed by Sandstrom *et al*(20) for HMBPP is able to interact with negatively charged small molecules, and strongly support, alongside the NMR chemical shift data, that this is indeed the site for P-Ag interaction. Although we were only able to co-crystallise the non-antigenic citrate and malonate molecules in complex with B30.2, the high quality electron density for both molecules in their respective structures provides the first glimpse of how such molecules can interact with the surrounding residues of the pocket. Although citrate and malonate clearly do not represent biologically relevant antigens for V γ 9V δ 2 T cells, importantly they unequivocally confirm the ability of the B30.2 electropositive pocket to interact with electronegative small molecules. Collectively our data firmly establish this pocket as the site for P-Ag interaction on B30.2.

Our findings have implications for the nature of the triggering mechanism that initiates P-Ag sensing, and for the means by which BTN3A1 is able to distinguish P-Ag from non-antigenic small molecules. Previously, a conformational change in the B30.2 domain was invoked as a likely consequence of P-Ag interaction, based on an earlier study by Hsiao *et al*(27) demonstrating chemical shift perturbations in the B30.2 domain on ligand binding, and the observation that soaking of cHDMAPP into apo B30.2 crystals caused them to dissolve unless they were previously cross-linked with glutaraldehyde (20). Our NMR data further strengthens this concept, as we can report exposure to P-Ag resulted in chemical shift perturbations to specific, identifiable residues both proximal and distal to the electropositive patch, suggesting a conformational change emanating from the P-Ag binding site. Distal residues that appear to be influenced include K366, Q369, F390, I391, S413, K419, N428, G429 and W431. Although in principle these distal shifts could have resulted from direct P-Ag interaction with the residues involved, this was extremely unlikely as rather than being clustered in a discrete site(s) on the structure, they were dispersed across its surface. In contrast to P-Ag mediated effects, although shifts were observed upon interaction with the non-antigens citrate/malonate, these were low in number, small in magnitude, and restricted

to residues close to the citrate/malonate moieties, consistent with binding but excluding such distal conformational alterations. Importantly, a number of these antigen-specific conformational alterations (K366, Q369 and K419) are involved in crystal contacts in the apo form of B30.2, consistent with the observation that P-Ag soaking dissolves such crystals. The lack of such changes upon citrate/malonate interaction is consistent with the observation that citrate/malonate-complexed structures of B30.2 closely match that of the apo form. ADP, a common cellular diphosphate, also interacted with the B30.2 and caused chemical shift perturbations distal to the proposed binding pocket. However the direction of these shifts differed to those observed with immunogenic P-Ags suggesting that a specific B30.2 conformation may be required to activate V γ 9/V δ 2 T cells. This model would predict that recent non-immunogenic ‘phosphoantagonist’ compounds(28) derived from modification of P-Ags are likely to competitively inhibit P-Ag-mediated V γ 9/V δ 2 T cell activation by binding to the same electropositive pocket on B30.2, but fail to induce the conformational change in B30.2 that results from HMBPP/IPP binding. Future studies could address this prediction.

Finally, the *in silico* docking simulations we carried out provide a biophysical rationalisation for small molecule interaction with B30.2. In addition to confirming that a negatively charged ‘head group’ is a key feature of ligands predicted to interact with the B30.2 ligand binding pocket, they highlight the potential importance of H381 in forming a hydrogen bonding interaction with the hydroxyl group of HMBPP. This is consistent with the critical importance of H381 in HMBPP sensing as highlighted by both Adams and Morita groups on the basis of mutational studies(20, 21), and suggest it could be a component of a conformational trigger. Although the details of such a mechanism remain unclear, in keeping with this suggestion, residues W380-Y382 were unassignable on NMR, suggesting considerable flexibility in this loop region in solution, and conversely chemical shifts were observed upon P-Ag exposure in residue V384, which was not predicted to interact directly with P-Ag in docking experiments. Furthermore, mutations to H381 significantly impaired the activation of V γ 9/V δ 2 T cells. In contrast to Shippy *et al* (29), whose model proposed an interaction between Y382 and P-Ag, we found that mutations to Y382 had differing effects on V γ 9/V δ 2 T cell activation, depending on the particular mutation, and our NMR data suggest that this is due to alterations in conformational change induced by P-Ags, which may be due to alterations in the P-Ag binding pocket.

In summary, our findings support the notion that a specific conformational change in the intracellular B30.2 domain of BTN3A1 is triggered as a direct result of P-Ag interaction, and that the ability to induce such a conformational change may be a key property that distinguishes antigenic small molecules capable of triggering V γ 9/V δ 2 T cell activation from other non-antigenic molecules that merely bind to B30.2. In doing so, they provide robust evidence that B30.2 acts as a ‘conformational sensor’ to detect intracellular P-Ag exposure. A limitation of the current study is that the nature of how this is transmitted to the cell exterior is unclear. There are various mechanisms conceivable, such as ‘inside-out’ propagation of conformational alterations (20), or alternatively recruitment of additional cell-surface proteins to the P-Ag-bound B30.2 domain. Additional structural and molecular studies on BTN3A1 may shed light on these issues. In addition, another poorly understood issue that warrants further investigation is how extracellular P-Ag can access intracellular

compartments, although energy dependent processes are clearly involved (30). However, as there is strong therapeutic interest in V γ 9/V δ 2 T cells, the current study will inform attempts to develop more potent V γ 9/V δ 2 T cell-based immunotherapies, including those directed against cancer, specifically highlighting the requirement for P-Ag to access intracellular compartments and to induce appropriate conformational alterations in BTN3A1. Successful exploitation of V γ 9/V δ 2 T cell recognition would complement current immunotherapy concepts focussed on $\alpha\beta$ T cell recognition that depend on MHC expression for efficacy, potentially enabling targeting of tumours where MHC downregulation is relatively common.

Methods

Cloning, expression and protein purification of BTN3A1-IgV and BTN3A1-B30.2 domains

Protein production for crystallization studies—The gene encoding the BTN3A1-B30.2 domain (R322-A513) was cloned into pET26 with a C-terminal His tag, and transformed into BL21 (DE3) competent *E. coli* cells (New England Biolabs). Transformed *E. coli* were cultured at 37°C until an OD₆₀₀ of 0.4-0.6 was attained. Protein expression was induced with 0.5 mM Isopropyl- β -D-1-Thiogalactopyranoside and cells were cultured for a further 18-20 hours at 18°C. The pelleted bacterial biomass was resuspended into 50mM Sodium phosphate pH 7.4, 500mM Sodium chloride, 50mM Imidazole, 0.5mM Tris (2-carboxyethyl) phosphine (TCEP) and Complete EDTA free protease inhibitors (Sigma-Aldrich) and homogenised using an AVESTIN EmulsiFlex C3 and centrifuged at 19000rpm/4°C for 30 minutes. The harvested supernatant was loaded onto a 5ml Hi-Trap column (GE) overnight. The column was washed with 5 column volumes of resuspension buffer to prevent non-specific binding. His-tagged protein was eluted with resuspension buffer containing a high concentration of imidazole (300mM) and further purified by size exclusion chromatography using a HiLoad 26/60 Superdex 200 column pre-equilibrated with 50mM Sodium Phosphate pH 7.4, 150mM Sodium Chloride, 0.5mM TCEP and Complete EDTA free protease inhibitors.

Protein production for Nuclear Magnetic Resonance spectroscopy studies—BTN3A1-IgV (S28-V143) and BTN3A1-B30.2 (R322-A513) constructs for NMR experiments were overexpressed in BL21 (DE3) *E. coli* in the presence of M9 minimal media supplemented with ¹⁵N labelled ammonium chloride, ¹³C labelled glucose and deuterated water. Further purification steps were followed as previously described. BTN3A1-IgV was purified by size exclusion chromatography into 20mM MES pH6.5, 50mM NaCl. BTN3A1-B30.2 was purified by size exclusion chromatography into a buffer containing 50mM Sodium Phosphate, 50mM Sodium Chloride, 0.5mM TCEP and Complete EDTA free protease inhibitors (pH 7.4).

Crystallization

BTN3A1-B30.2 domain was concentrated with tenfold excess cHDMAPP (Cayman Chemical) to 20mg/ml and subjected to crystallisation trials with the mosquito robot (TTpLabTech) using the hanging-drop vapour diffusion method. Diffraction-grades crystals were grown in drops equilibrated against Index (Hampton Research) condition 88 (0.2M

Ammonium Citrate tribasic [pH 7.0], 20% w/v Polyethylene glycol (PEG) 3,350 [pH 7.0] and JCSG-*plus* (Molecular Dimensions) condition 78 (0.2M Sodium malonate dibasic monohydrate [pH 7.0], 20% w/v PEG 3,350). Crystals appeared after 5 days at 298K. Prior to data collection crystals were soaked in mother liquor supplemented with increasing concentrations of ethylene glycol (10, 20 and 25%) and flash cooled in liquid nitrogen gas stream. X-ray diffraction data sets were collected to 1.7Å (BTN3A1-B30.2-citrate) using the 'in house' X-ray diffraction facility and at 1.6Å (BTN3A1-B30.2-malonate) at the Diamond Light Source (beamline I02). X-ray data were integrated and scaled using programs of the XDS suite (31).

Structural Determination

The structures were determined using the molecular replacement phasing method with MOLREP (32). The previously resolved structure of the BTN3A1-B30.2 domain was used as a search model (pdb code 4N7I; Sandstrom et al). Model building and refinement were performed in COOT (33) and REFMAC5 (34), respectively. Water molecules were added iteratively to each model, followed by cycles of refinement. The data collection and refinement statistics are summarised in Table S1. The stereochemical quality of the atomic models was assessed using PROCHECK (35). Ribbon diagrams and molecular surface representations were generated by PyMol (36). The atomic co-ordinates and structure factors have been deposited on the Protein Data Bank with accession codes (5LYG (BTN3A1-B30.2-malonate) and 5LYK (BTN3A1-B30.2-citrate)).

Nuclear Magnetic Resonance Spectroscopy

NMR experiments were performed on 600MHz and 900MHz Oxford Avance III spectrometers equipped with TXO (600MHz) and TCI (900MHz) 5mm z-pulse field gradient triple enhanced cryogenic probes at 298 K. Sequential assignments were made from TROSY versions of HN(CO)CA, HNCA, HN(CO)CACB, HNCACB, HN(CA)CO and HNCO experiments with non-uniform sampling (37–39). Phosphoantigen titration experiments with BTN3A1-IgV (0.3mM) and BTN3A1-B30.2 (0.3 mM) were performed by Heteronuclear Single Quantum Coherence spectroscopy (HSQC) using 1.5 mM IPP (Teu Bio), 1.5 mM HMBPP (Teu Bio) and 1.5 mM cHDMAPP (Cayman Chemicals). Malonate and Citrate titrations were performed using 100mM as this was reflective of the relative conditions found in the crystallization conditions. The data was acquired using Topspin 3.2.6 (Bruker), the spectra were processed using NMRPipe (40) and were analysed using SPARKY(41).

T cell isolation, culture and activation

Human peripheral blood mononuclear cells (PBMC) were isolated from heparinised venous blood from consented healthy donors (protocol approved by the NRES Committee West Midlands ethical board; REC reference 14/WM/1254). Briefly, whole blood was layered over lymphoprep© (Stem Cell Technologies) and centrifuged with resulting PBMC used for subsequent experiments. 5×10^5 PBMC were cultured for 20 hours in the presence of medium alone, medium supplement with vehicle (DMSO; Sigma) or medium supplemented with the indicated concentrations of cHDMAPP, IPP, ammonium citrate and sodium malonate. The cell culture medium used was RPMI-1640 media supplemented with 2 mM

L-glutamine, 1% sodium pyruvate, 50 µg/ml penicillin/streptomycin (Invitrogen) and 10% fetal calf serum (Sigma). Vδ2⁺ T cells were expanded from PBMCs with 5µM Zoledronate (Sigma) and subsequent addition of 100 units/mL IL-2 (Biolegend) every three days. Cultured PBMC were labelled with aqua viability dye (Biolegend), and then cells were stained for surface antigens with antibodies directed against CD3 (UCHT1), CD8 (SK1), CD69 (FN50), CD25 (2A3); all Biolegend, TCR Vγ9 (IMMU360); Beckman Coulter, and TCR Vδ2 (123R3); Miltenyi. Cells were acquired on an LSR II (Beckton Dickinson) and data analysed with FlowJo V10.1 (TreeStar). Tabulated data were analysed and graphed in Graphpad PRISM 7 (Graphpad Software Inc).

Generation of BTN3A1 B30.2 mutants

Site directed mutagenesis was performed on both eukaryotic and mammalian expression vectors using Q5® High-Fidelity DNA Polymerase (New England Biolabs) according to the manufacturer's instructions. Primers used can be found in Table S2.

Overexpression of Mutant BTN3A1 and Co-culture assays

Wildtype and mutant forms of BTN3A1 were reintroduced into BTN3A1 KO HEK293T cells at 0.5µg DNA in a transfection mix containing 0.1 mg/mL polyethylenimine supplemented with serum free OptiMem (Invitrogen). Transfected cells were treated with 10µM Zoledronate for 24 hours and HEK293T cells were then co-cultured for a further 18 hours with expanded human Vδ2⁺ T cells at a ratio of 1:1. Cells were then labelled with aqua viability dye and stained with antibodies directed against the cell surface markers CD3 (UCHT1), TCR Vγ9 (IMMU360), TCR Vδ2 (123R3), and CD25 (2A3).

Molecular modelling studies

The computational studies were executed by the PC windows 7 with Intel Core i7-4790 / 3.6GHz microprocessor, 16 GB RAM and 64 Bit operating system. Molecular docking was performed using different tools provided by OpenEye Scientific Software (<http://www.eyesopen.com>). The three-dimensional crystal structure of the intracellular B30.2 domain of BTN3A1 in complex with cHDMAPP was retrieved from the Protein Data Bank (PDB ID: 4N7U). This was used as the receptor and the active site was identified on the basis of the bound ligand. Omega2 (OpenEye Scientific Software) was used to generate multiple ligand conformers using the default settings (42). FRED (fast rigid exhaustive docking) rigidly fitted these conformers into the pre-defined binding site and ranks the poses by scoring functions (43, 44). The VIDA module of the OpenEye toolkit was then used to visualise the docked poses within the receptor's active site and to inspect the docked poses as well as identify the main interacting residues.

Supplementary Material

Refer to Web version on PubMed Central for supplementary material.

Acknowledgements

We thank the Henry Wellcome Building for Biomolecular NMR Spectroscopy for access and support, and the University of Birmingham Protein Expression Facility and the University of Birmingham Macromolecular X-ray

Diffraction Facility for use of their facilities. The authors would like to thank Diamond Light Source for beamtime (proposal mx14692), and the staff of beamline I04 for assistance with remote data collection.

Funding Sources

The work was supported by Wellcome Trust Investigator award funding to BEW, supporting MSD, CRW, FM, and MS (Grant code: 364 099266/Z/12/Z).

References

1. Morita CT, Jin C, Sarikonda G, Wang H. Nonpeptide antigens, presentation mechanisms, and immunological memory of human Vgamma2Vdelta2 T cells: discriminating friend from foe through the recognition of prenyl pyrophosphate antigens. *Immunol Rev.* 2007; 215:59–76. [PubMed: 17291279]
2. Dimova T, Brouwer M, Gosselin F, Tassignon J, Leo O, Donner C, Marchant A, Vermijlen D. Effector Vgamma9Vdelta2 T cells dominate the human fetal gammadelta T-cell repertoire. *Proc Natl Acad Sci U S A.* 2015; 112:E556–565. [PubMed: 25617367]
3. Shen Y, Zhou D, Qiu L, Lai X, Simon M, Shen L, Kou Z, Wang Q, Jiang L, Estep J, Hunt R, et al. Adaptive immune response of Vgamma2Vdelta2+ T cells during mycobacterial infections. *Science.* 2002; 295:2255–2258. [PubMed: 11910108]
4. Allison TJ, Winter CC, Fournie JJ, Bonneville M, Garboczi DN. Structure of a human gammadelta T-cell antigen receptor. *Nature.* 2001; 411:820–824. [PubMed: 11459064]
5. De Libero G, Casorati G, Giachino C, Carbonara C, Migone N, Matzinger P, Lanzavecchia A. Selection by two powerful antigens may account for the presence of the major population of human peripheral gamma/delta T cells. *J Exp Med.* 1991; 173:1311–1322. [PubMed: 1827824]
6. Morita CT, Beckman EM, Bukowski JF, Tanaka Y, Band H, Bloom BR, Golan DE, Brenner MB. Direct presentation of nonpeptide prenyl pyrophosphate antigens to human gamma delta T cells. *Immunity.* 1995; 3:495–507. [PubMed: 7584140]
7. Davey MS, Lin CY, Roberts GW, Heuston S, Brown AC, Chess JA, Toleman MA, Gahan CG, Hill C, Parish T, Williams JD, et al. Human neutrophil clearance of bacterial pathogens triggers antimicrobial gammadelta T cell responses in early infection. *PLoS Pathog.* 2011; 7:e1002040. [PubMed: 21589907]
8. Gober HJ, Kistowska M, Angman L, Jenö P, Mori L, De Libero G. Human T cell receptor gammadelta cells recognize endogenous mevalonate metabolites in tumor cells. *J Exp Med.* 2003; 197:163–168. [PubMed: 12538656]
9. Fisher JP, Heuvelink J, Yan M, Gustafsson K, Anderson J. gammadelta T cells for cancer immunotherapy: A systematic review of clinical trials. *Oncoimmunology.* 2014; 3:e27572. [PubMed: 24734216]
10. Tanaka Y, Morita CT, Tanaka Y, Nieves E, Brenner MB, Bloom BR. Natural and synthetic non-peptide antigens recognized by human gamma delta T cells. *Nature.* 1995; 375:155–158. [PubMed: 7753173]
11. Hintz M, Reichenberg A, Altincicek B, Bahr U, Gschwind RM, Kollas AK, Beck E, Wiesner J, Eberl M, Jomaa H. Identification of (E)-4-hydroxy-3-methyl-but-2-enyl pyrophosphate as a major activator for human gammadelta T cells in *Escherichia coli*. *FEBS Lett.* 2001; 509:317–322. [PubMed: 11741609]
12. Fisch P, Malkovsky M, Braakman E, Sturm E, Bolhuis RL, Prieve A, Sosman JA, Lam VA, Soudel PM. Gamma/delta T cell clones and natural killer cell clones mediate distinct patterns of non-major histocompatibility complex-restricted cytotoxicity. *J Exp Med.* 1990; 171:1567–1579. [PubMed: 2185329]
13. Dieli F, Gebbia N, Poccia F, Caccamo N, Montesano C, Fulfaro F, Arcara C, Valerio MR, Meraviglia S, Di Sano C, Sireci G, et al. Induction of gammadelta T-lymphocyte effector functions by bisphosphonate zoledronic acid in cancer patients in vivo. *Blood.* 2003; 102:2310–2311. [PubMed: 12959943]
14. Kunzmann V, Bauer E, Feurle J, Weissinger F, Tony HP, Wilhelm M. Stimulation of gammadelta T cells by aminobisphosphonates and induction of antiplasma cell activity in multiple myeloma. *Blood.* 2000; 96:384–392. [PubMed: 10887096]

15. Luckman SP, Hughes DE, Coxon FP, Graham R, Russell G, Rogers MJ. Nitrogen-containing bisphosphonates inhibit the mevalonate pathway and prevent post-translational prenylation of GTP-binding proteins, including Ras. *J Bone Miner Res.* 1998; 13:581–589. [PubMed: 9556058]
16. Harly C, Guillaume Y, Nedellec S, Peigne CM, Monkkinen H, Monkkinen J, Li J, Kuball J, Adams EJ, Netzer S, Dechanet-Merville J, et al. Key implication of CD277/butyrophilin-3 (BTN3A) in cellular stress sensing by a major human gammadelta T-cell subset. *Blood.* 2012; 120:2269–2279. [PubMed: 22767497]
17. Vavassori S, Kumar A, Wan GS, Ramanjaneyulu GS, Cavallari M, El Daker S, Beddoe T, Theodossis A, Williams NK, Gostick E, Price DA, et al. Butyrophilin 3A1 binds phosphorylated antigens and stimulates human gammadelta T cells. *Nat Immunol.* 2013; 14:908–916. [PubMed: 23872678]
18. Palakodeti A, Sandstrom A, Sundaresan L, Harly C, Nedellec S, Olive D, Scotet E, Bonneville M, Adams EJ. The molecular basis for modulation of human Vgamma9Vdelta2 T cell responses by CD277/butyrophilin-3 (BTN3A)-specific antibodies. *J Biol Chem.* 2012; 287:32780–32790. [PubMed: 22846996]
19. Rhodes DA, Chen HC, Price AJ, Keeble AH, Davey MS, James LC, Eberl M, Trowsdale J. Activation of human gammadelta T cells by cytosolic interactions of BTN3A1 with soluble phosphoantigens and the cytoskeletal adaptor periplakin. *J Immunol.* 2015; 194:2390–2398. [PubMed: 25637025]
20. Sandstrom A, Peigne CM, Leger A, Crooks JE, Konczak F, Gesnel MC, Breathnach R, Bonneville M, Scotet E, Adams EJ. The intracellular B30.2 domain of butyrophilin 3A1 binds phosphoantigens to mediate activation of human Vgamma9Vdelta2 T cells. *Immunity.* 2014; 40:490–500. [PubMed: 24703779]
21. Wang H, Morita CT. Sensor Function for Butyrophilin 3A1 in Prenyl Pyrophosphate Stimulation of Human Vgamma2Vdelta2 T Cells. *J Immunol.* 2015; 195:4583–4594. [PubMed: 26475929]
22. Boedec A, Sicard H, Dessolin J, Herbette G, Ingoure S, Raymond C, Belmant C, Kraus JL. Synthesis and biological activity of phosphonate analogues and geometric isomers of the highly potent phosphoantigen (E)-1-hydroxy-2-methylbut-2-enyl 4-diphosphate. *J Med Chem.* 2008; 51:1747–1754. [PubMed: 18303828]
23. de Bruin RC, Stam AG, Vangone A, van Bergen En Henegouwen PM, Verheul HM, Sebestyen Z, Kuball J, Bonvin AM, de Gruijl TD, van der Vliet HJ. Prevention of Vgamma9Vdelta2 T Cell Activation by a Vgamma9Vdelta2 TCR Nanobody. *J Immunol.* 2017; 198:308–317. [PubMed: 27895170]
24. Eberl M, Roberts GW, Meuter S, Williams JD, Topley N, Moser B. A rapid crosstalk of human gammadelta T cells and monocytes drives the acute inflammation in bacterial infections. *PLoS Pathog.* 2009; 5:e1000308. [PubMed: 19229322]
25. Rincon-Orozco B, Kunzmann V, Wrobel P, Kabelitz D, Steinle A, Herrmann T. Activation of V gamma 9V delta 2 T cells by NKG2D. *J Immunol.* 2005; 175:2144–2151. [PubMed: 16081780]
26. Rhodes DA, Reith W, Trowsdale J. Regulation of Immunity by Butyrophilins. *Annu Rev Immunol.* 2016; 34:151–172. [PubMed: 26772212]
27. Hsiao CH, Lin X, Barney RJ, Shippy RR, Li J, Vinogradova O, Wiemer DF, Wiemer AJ. Synthesis of a phosphoantigen prodrug that potently activates Vgamma9Vdelta2 T-lymphocytes. *Chem Biol.* 2014; 21:945–954. [PubMed: 25065532]
28. Espinosa E, Belmant C, Sicard H, Poupot R, Bonneville M, Fournie JJ. Y2K+1 state-of-the-art on non-peptide phosphoantigens, a novel category of immunostimulatory molecules. *Microbes Infect.* 2001; 3:645–654. [PubMed: 11445451]
29. Shippy RR, Lin X, Agabiti SS, Li J, Zangari BM, Foust BJ, Poe MM, Hsiao CC, Vinogradova O, Wiemer DF, Wiemer AJ. Phosphinophosphonates and Their Tris-pivaloyloxymethyl Prodrugs Reveal a Negatively Cooperative Butyrophilin Activation Mechanism. *J Med Chem.* 2017; 60:2373–2382. [PubMed: 28218845]
30. Kilcollins AM, Li J, Hsiao CH, Wiemer AJ. HMBPP Analog Prodrugs Bypass Energy-Dependent Uptake To Promote Efficient BTN3A1-Mediated Malignant Cell Lysis by Vgamma9Vdelta2 T Lymphocyte Effectors. *J Immunol.* 2016; 197:419–428. [PubMed: 27271567]
31. Kabsch W. Xds. *Acta Crystallogr D Biol Crystallogr.* 2010; 66:125–132. [PubMed: 20124692]

32. Vagin A, Teplyakov A. Molecular replacement with MOLREP. *Acta Crystallogr D Biol Crystallogr.* 2010; 66:22–25. [PubMed: 20057045]
33. Emsley P, Cowtan K. Coot: model-building tools for molecular graphics. *Acta Crystallogr D Biol Crystallogr.* 2004; 60:2126–2132. [PubMed: 15572765]
34. Murshudov GN, Skubak P, Lebedev AA, Pannu NS, Steiner RA, Nicholls RA, Winn MD, Long F, Vagin AA. REFMAC5 for the refinement of macromolecular crystal structures. *Acta Crystallogr D Biol Crystallogr.* 2011; 67:355–367. [PubMed: 21460454]
35. Laskowski RA, MacArthur MW, Moss DS, Thornton JM. PROCHECK: a program to check the stereochemical quality of protein structures. *J Appl Crystallogr.* 1993; 26:283–291.
36. Schrödinger L. The PyMOL Molecular Graphics System, Version 1.8.
37. Grzesiek S, Bax A. The Origin and Removal of Artifacts in 3D HACO Spectra of Proteins Uniformly Enriched with ^{13}C . *J Magn Reson, Ser B.* 1993; 102:103–106.
38. Kay LE, Xu GY, Singer AU, Muhandiram DR, Formankay JD. A gradient-enhanced HCCH-TOCSY experiment for recording side-chain ^1H and ^{13}C correlations in H_2O samples of proteins. *J Magn Reson, Ser B.* 1993; 101:333–337.
39. Muhandiram DR, Kay LE. Gradient-Enhanced Triple-Resonance Three-Dimensional NMR Experiments with Improved Sensitivity. *J Magn Reson, Ser B.* 1994; 103:203–216.
40. Delaglio F, Grzesiek S, Vuister GW, Zhu G, Pfeifer J, Bax A. NMRPipe: a multidimensional spectral processing system based on UNIX pipes. *J Biomol NMR.* 1995; 6:277–293. [PubMed: 8520220]
41. Goddard, TD, Kneller, DG. Sparky 3. University of California; San Francisco: 2001.
42. Hawkins PC, Nicholls A. Conformer generation with OMEGA: learning from the data set and the analysis of failures. *J Chem Inf Model.* 2012; 52:2919–2936. [PubMed: 23082786]
43. McGann M. FRED pose prediction and virtual screening accuracy. *J Chem Inf Model.* 2011; 51:578–596. [PubMed: 21323318]
44. McGann MR, Almond HR, Nicholls A, Grant JA, Brown FK. Gaussian docking functions. *Biopolymers.* 2003; 68:76–90. [PubMed: 12579581]

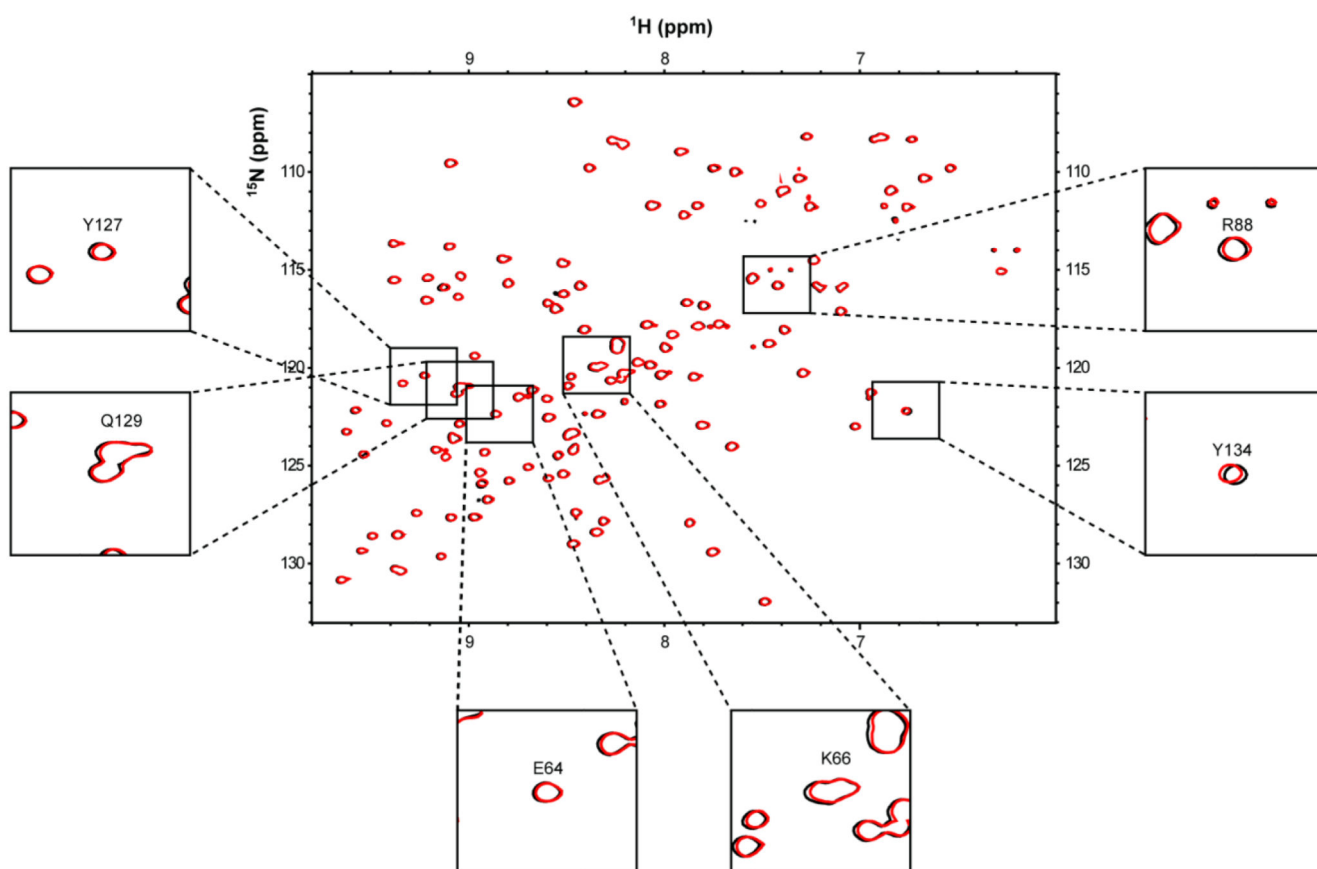


Figure 1. NMR chemical shift perturbation analysis of BTN3A1-IgV domain with HMBPP. Overlay of ^1H ^{15}N HSQC spectra of ^{15}N -labelled 0.3mM BTN3A1-IgV domain in the absence (black) and presence (red) of 1.5 mM HMBPP. The black boxes highlight a close-up view of peaks corresponding to BTN3A1-IgV residues (E64, K66, R88, Y127, Q129 and Y134) that have previously been implicated in binding HMBPP based on X-ray crystallographic data.

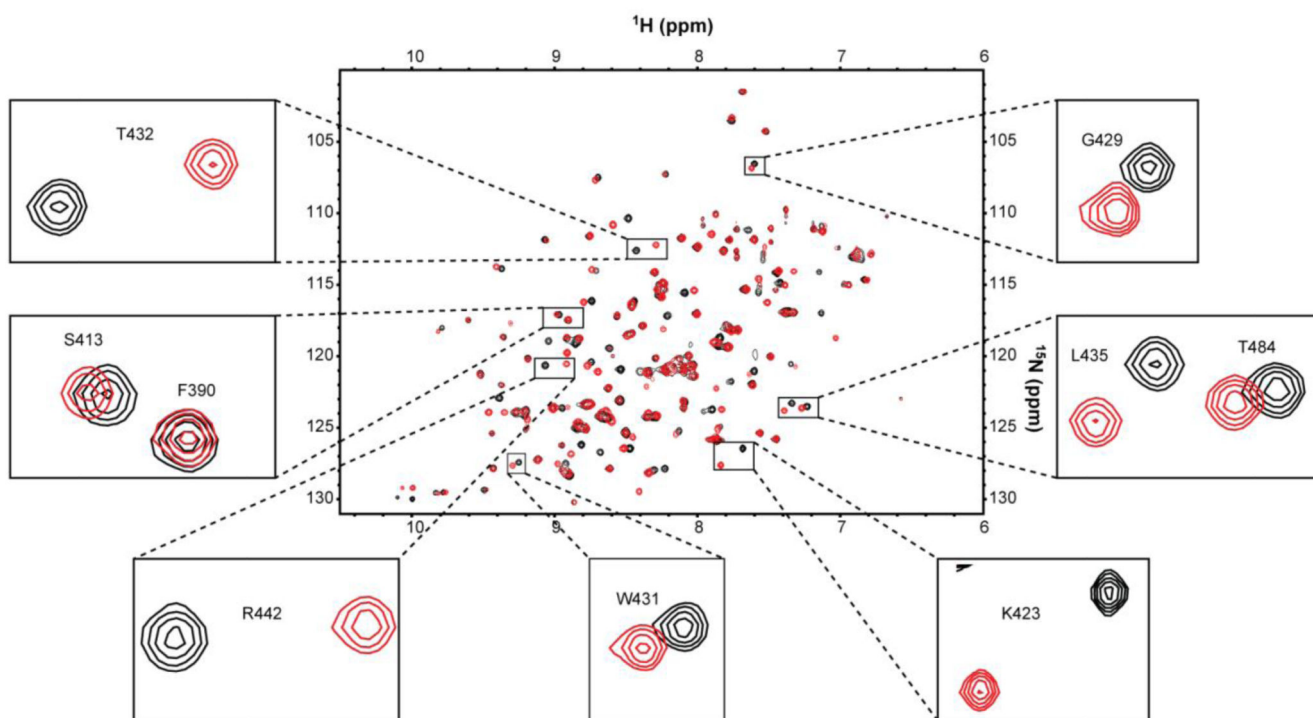


Figure 2. NMR chemical shift perturbation analysis of BTN3A1-B30.2 intracellular domain with cHDMAPP.

Overlay of ^1H ^{15}N HSQC spectra of ^{15}N -labelled 0.3 mM BTN3A1-B30.2 domain in the absence (black) and presence (red) of non-labelled 3mM cHDMAPP. The black boxes highlight a close-up view of peaks corresponding to selected BTN3A1-B30.2 residues that undergo chemical shift perturbation following titration with cHDMAPP (examples include small (S413), medium (G429) and large (T432, R442 and K423) chemical shift perturbations).

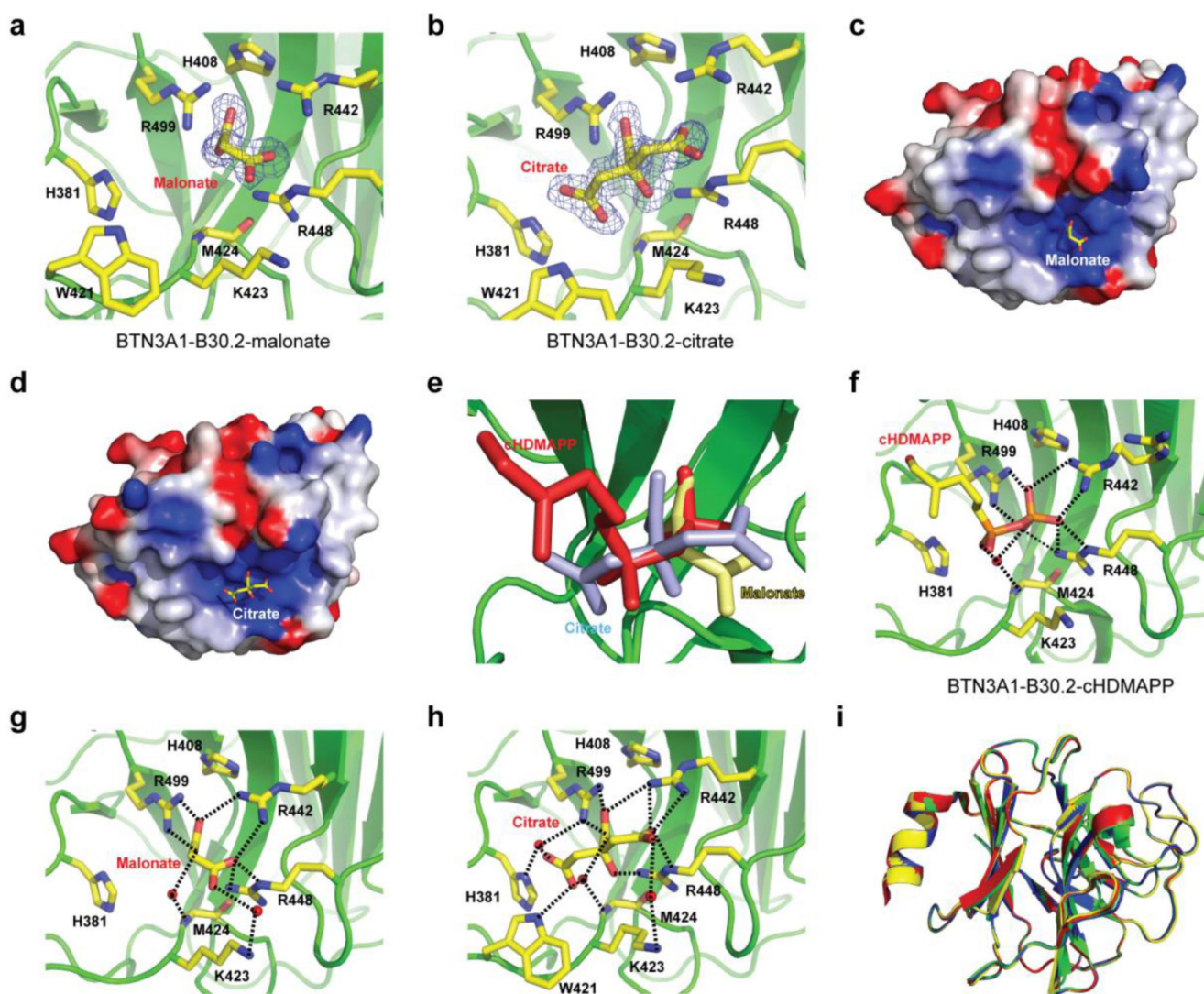


Figure 3. Structural analysis of BTN3A1-B30.2 in complex with malonate and citrate.

a) BTN3A1-B30.2-malonate complex with the 1.4Å resolution composite omit Fo-Fc electron density map for malonate contoured at 2σ (blue). b) BTN3A1-B30.2-citrate complex with the 1.7Å resolution composite omit Fo-Fc electron density map for malonate contoured at 2σ (blue). Residues in close proximity to malonate or citrate are shown (ball and stick format). c) Electrostatic potential of the BTN3A1-B30.2-malonate complex calculated with DelPhi with the potential scale ranging from -7 (red) to +7 (blue) in units of kT/e . d) Electrostatic potential of the BTN3A1-B30.2-citrate complex calculated with DelPhi with the potential scale ranging from -7 (red) to +7 (blue) in units of kT/e . e) BTN3A1-B30.2 binding pocket (green) with the structures of malonate (yellow), citrate (blue) and cHDMAPP (red) superimposed. f-h) Structures of BTN3A1-B30.2 bound to cHDMAPP (f), malonate (g) and citrate (h). I) Superimposition of the $C\alpha$ backbones for BTN3A1-B30.2 (green), BTN3A1-B30.2-malonate complex (yellow), BTN3A1-B30.2-citrate complex (blue) and BTN3A1-B30.2-cDHAMPP complex (red). BTN3A1-B30.2

residues that mediate hydrogen bonding interactions (black dashed lines) with each ligand are shown (ball and stick format). Red spheres represent water molecules.

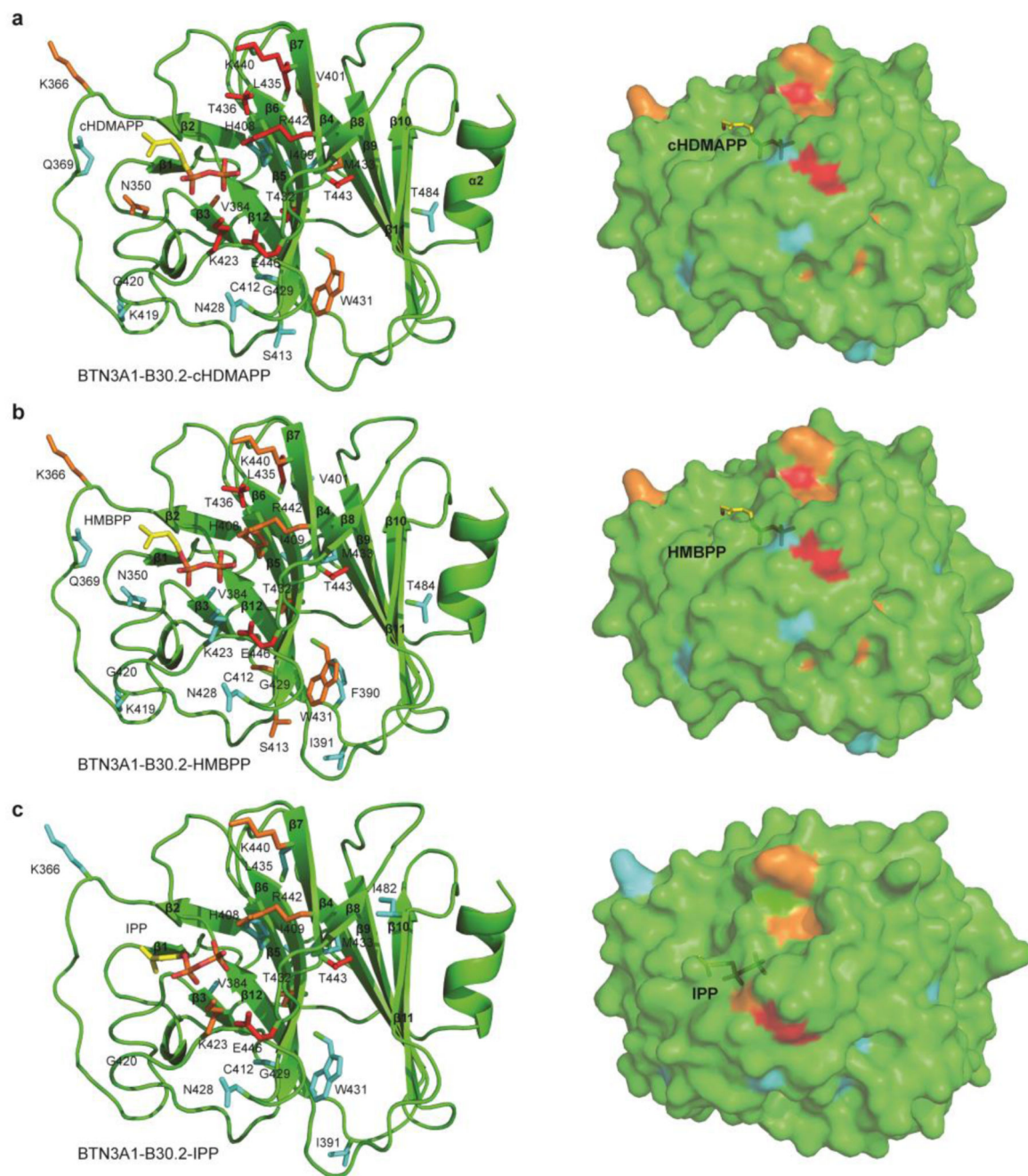


Figure 4. Chemical shift perturbation mapping of the cHDMAPP, HMBPP and IPP binding sites on BTN3A1-B30.2 domain.

a) Surface mapping of perturbed residues of BTN3A1-B30.2 (shown as stick format) upon cHDMAPP binding. Residues are coloured based on small (cyan), medium (orange) and large (red) chemical shift perturbations. cHDMAPP is shown as stick format. b) Surface mapping of perturbed residues of BTN3A1-B30.2 (shown as stick format) upon HMBPP binding. Residues are coloured based on small (cyan), medium (orange) and large (red) chemical shift perturbations. HMBPP is shown as stick format. c) Surface mapping of perturbed residues of BTN3A1-B30.2 (shown as stick format) upon IPP binding. Residues

are coloured based on small (cyan), medium (orange) and large (red) chemical shift perturbations. IPP is shown as stick format.

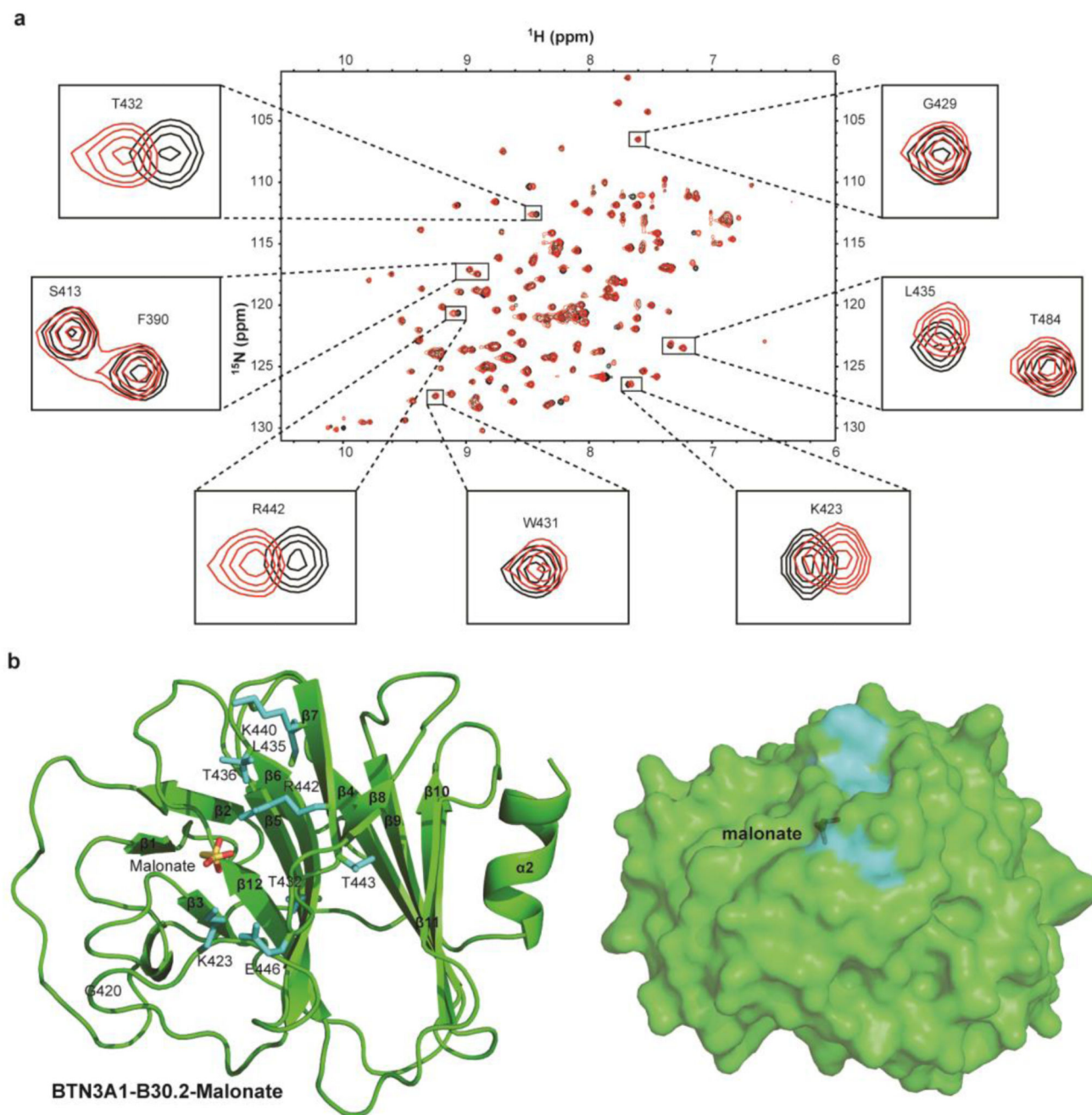


Figure 5. NMR chemical shift perturbation analysis of BTN3A1-B30.2 domain with malonate. a) Overlay of ^1H ^{15}N HSQC spectra of ^{15}N -labelled 0.3mM BTN3A1-B30.2 domain in the absence (black) and presence of 100mM sodium malonate (red). Black boxes highlight a close-up view of peaks corresponding to BTN3A1-B30.2 residues that undergo chemical shifts upon HMBPP/cHDMAPP binding. b) Surface mapping of perturbed residues of B30.2 (shown as stick format) upon malonate binding. Residues are coloured based on small (cyan), medium (orange) and large (red) chemical shift perturbations. Malonate is shown as stick format.

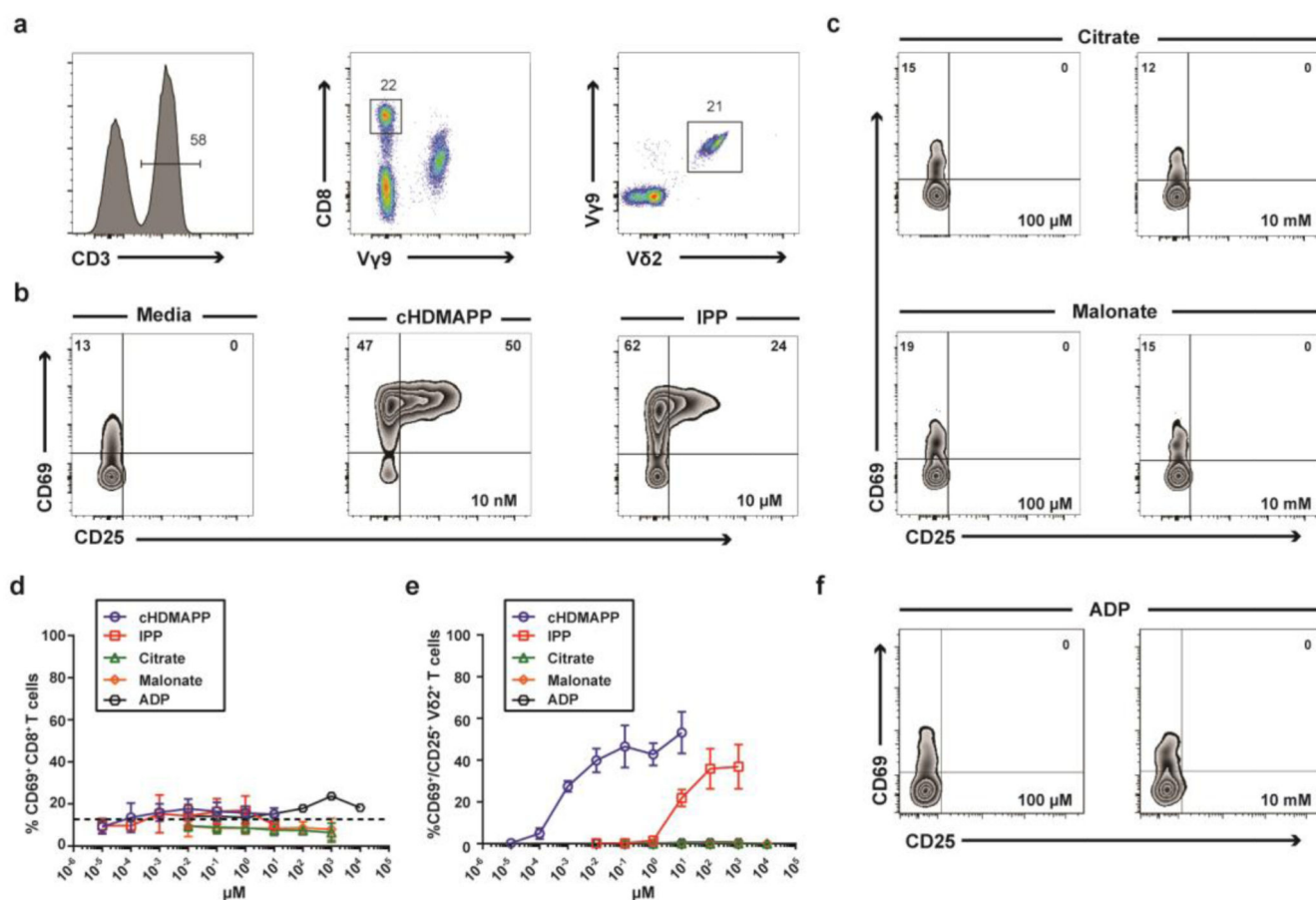


Figure 6. B30.2 domain of human BTN3A1 selectively binds small negatively charged moieties but only a limited set of these molecules directly activates human $V\gamma 9/V\delta 2^+$ T cells.

a) PBMCs were stained with antibodies directed against surface antigens for CD3, TCR $V\gamma 9$, TCR $V\delta 2$ and CD8. (n=3). b) PBMCs were incubated for 20 hours with the indicated concentration of P-Ags or medium and $V\gamma 9/V\delta 2^+$ T cells were assessed for the expression of CD69 and CD25. c) As in b), but PBMCs incubated with the indicated concentrations of the B30.2 binding molecules citrate and malonate. d) CD8⁺ T cells were assessed for the upregulation of CD69 following titration with indicated compounds. e) $V\gamma 9/V\delta 2^+$ T cells were assessed for the upregulation of CD69 and CD25 following titration with indicated compounds. Error bars indicate means \pm SEM.

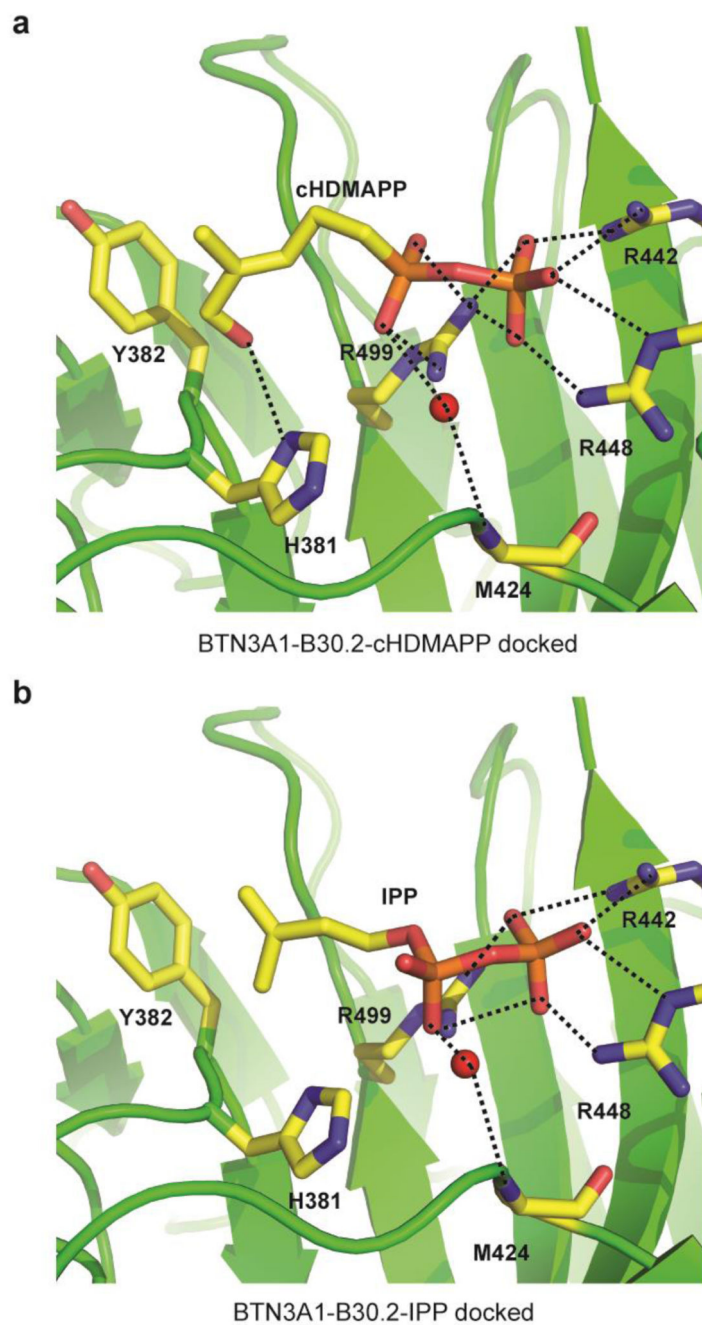


Figure 7. In silico docking of small molecule B30.2 domain binders.

a-b) Docking of cHDMAPP (a) and IPP (b), into the apo B30.2 domain structure showing important hydrogen bonding interactions (dashed black lines) with three key arginine residues (R442, R448 and R499). The hydroxyl group of cHDMAPP also mediates an additional hydrogen bonding interaction with H381. Red spheres represent water molecules.

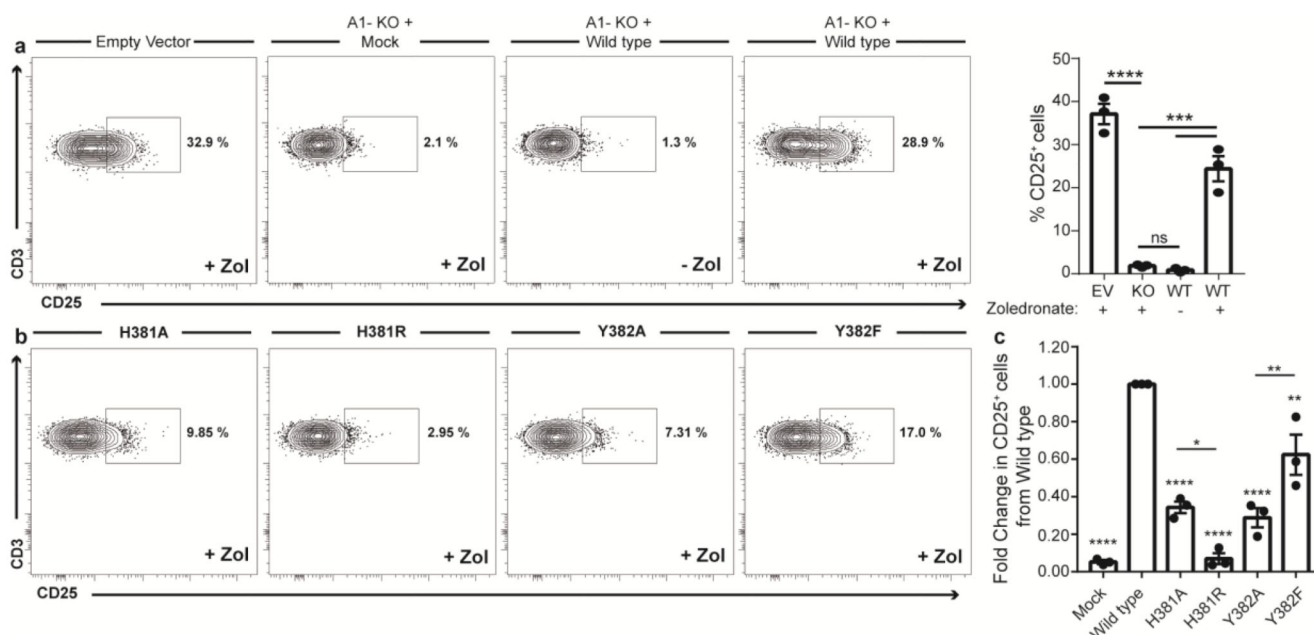


Figure 8. Mutations of BTN3A1-B30.2 H381 and Y382 residues abrogate $V\gamma 9^+/V\delta 2^+$ T cell activation.

(a) Representative and summary data from expanded human $V\delta 2^+$ T cells incubated in the presence of HEK293T cells subjected to an empty vector (Ev) or BTN3A1 CRISP/Cas9 (BTN3A1-KO) construct and then transiently transfected with BTN3A1 Wild Type construct pulsed with 10 μM zoledronate or medium and assessed for CD25 expression. (b) Representative and summary data from expanded human $V\delta 2^+$ T cells assessed for CD25 expression after incubation with BTN3A1-KO HEK293T cells transiently transfected with H381 and Y382 mutant BTN3A1 constructs and pulsed with 10 μM zoledronate. Summary data in (b), depicts each mutant and mock control CD25⁺ expression levels on $V\delta 2^+$ T cells normalised to the total CD25⁺ expression obtained for wild type BTN3A1 activation. $n = 3$. Error bars indicate means \pm SEM; ns = not significant, * $P < 0.05$; ** $P < 0.01$; *** $P < 0.001$, **** $P < 0.001$; p-values were determined by one-way ANOVA with Tukey's post hoc testing.